Electronic Supplementary Material (ESI) for Journal of Materials Chemistry C.

Supporting Information

Ferroelectric Low-Voltage ON/OFF Switching of Chiral Benzene-1,3,5-tricarboxamide Derivative

Jianyun Wu, Takashi Takeda, Norihisa Hoshino, and Tomoyuki Akutagawa

Contents

Experimental

General and physical measurements. Chiral ***S*-3BC** was synthesized from 1,3,5-benzenetricarbonyl trichloride and homochiral (*S*)-3,7-dimethyloctylamine according to the literature (Anal. Calcd. for $C_{39}H_{69}N_3O_3$: C, 74.59; H, 11.08; N, 6.69. Found: C, 74.37; H, 11.28; N, 6.67).[S1,S2] Solid state infrared (IR, 400–4000 cm^{-1}) spectra were measured in KBr pellets using a Thermo Fisher Scientific Nicolet 6700 spectrophotometer with a resolution of 4 cm^{-1}. Thermogravimetry–differential thermal analysis (TG-DTA) was carried out using a Rigaku Thermo Plus TG8120 thermal analysis station using an Al_2O_3 reference in the temperature range above 300 K with a heating rate of 5 K min^{-1} under N_2. Differential scanning calorimetry (DSC) analyses were carried out using METTLER DSC1-TS using an Al_2O_3 reference and a heating and cooling rate of 5 K min^{-1} under nitrogen. Temperature-dependent powder X-ray diffraction patterns (PXRD) were obtained using a Rigaku Rint-Ultima III diffractometer with Cu K_α radiation at λ = 1.54187 Å in the temperature range of 200 to 340 K. The temperature-dependent dielectric constants were measured using the two-probe AC impedance method in a frequency range from 1 kHz to 1 MHz (Hewlett-Packard, HP4194A) in a Linkam-LTS350 temperature control system. The *P*−*E* curve was measured using a ferroelectric tester (Precision LC, Radiant Technologies). The cast films were fabricated on indium tin oxide (ITO) glass (SZ-A311P6N) substrates, which were sandwiched together with a corresponding ITO glass. The electrode area and gap were 1 cm^2 and 2 μm, respectively.

References

S1) Brunsveld, L.; Schenning, A. P. H. J.; Broeren, M. A. C.; Janssen, H. M.; Vekemans, J. A. J. M.; Meijer, E. W. Chiral Amplification in Columns of Self-Assembled *N*,*N*',*N*"-Tris((*S*)-3,7-dimethyloctyl)benzene-1,3,5-tricarboxamide in Dilute Solution, *Chem. Lett*. **2000**, 292–293.

S2) Wilson, A. J.; Masuda, M.; Sijbesma, R. P. Meijer, E. W. Chiral Amplification in the Transcription of Supramolecular Helicity into a Polymer Backbone. *Angew. Chem., Int. Ed*. **2005**, *44*, 2275–2279.

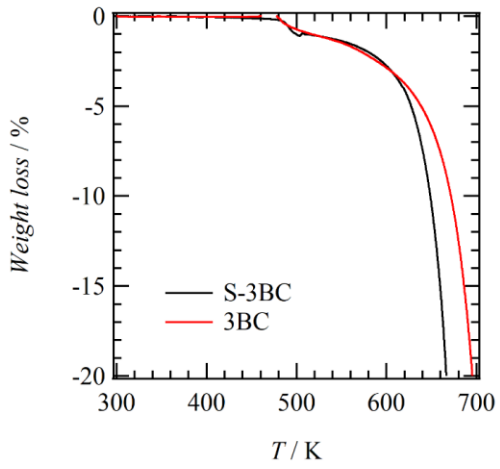

Figure S1. TG charts of **3BC** and ***S*-3BC**.

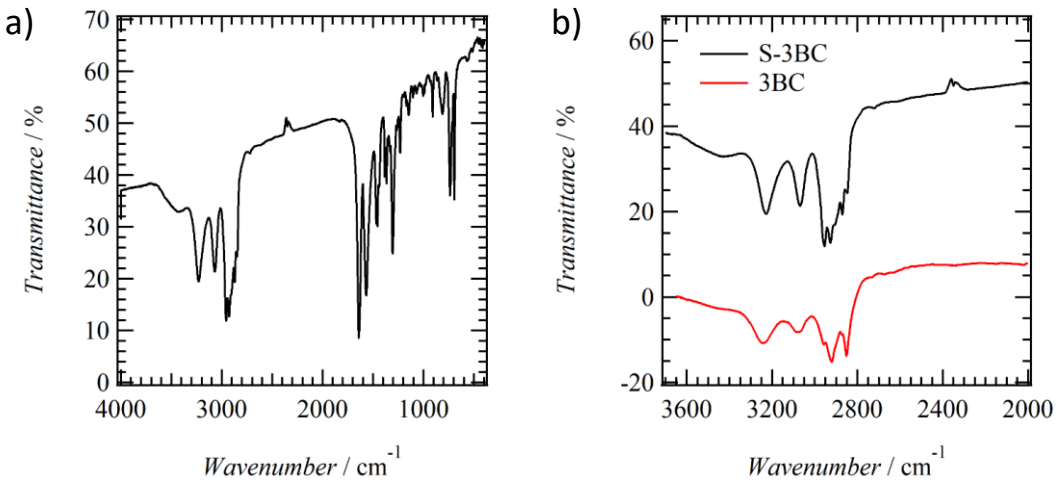

Figure S2. IR spectra of **3BC** and ***S*-3BC** at KBr pellets. Energy range at a) 400 ~ 4000 cm^{-1} and b) 2000 ~ 3700 cm^{-1}.

Table S1. Organogellation ability of ***S*-3BC** in the organic solvents.

Solvent	**3BC**	***S*-3BC**
m.p., K	467	514
Ethanol	OG	L
Acetonitrile	OG	TG
Acetone	OG	OG
Hexane	TG	×
Benzene	L	TG
Toluene	L	TG
Cyclohexane	L	TG
Chloroform	L	L
DMF	OG	L
DMSO	OG	OG
1, 2-Dichloroehtane	OG	×

a) Concentration was fixed at 20 mM. Notations of ×, L, OG, and TG corresponded to the insoluble, soluble, opaque organogel, and transparent organogel, respectively.

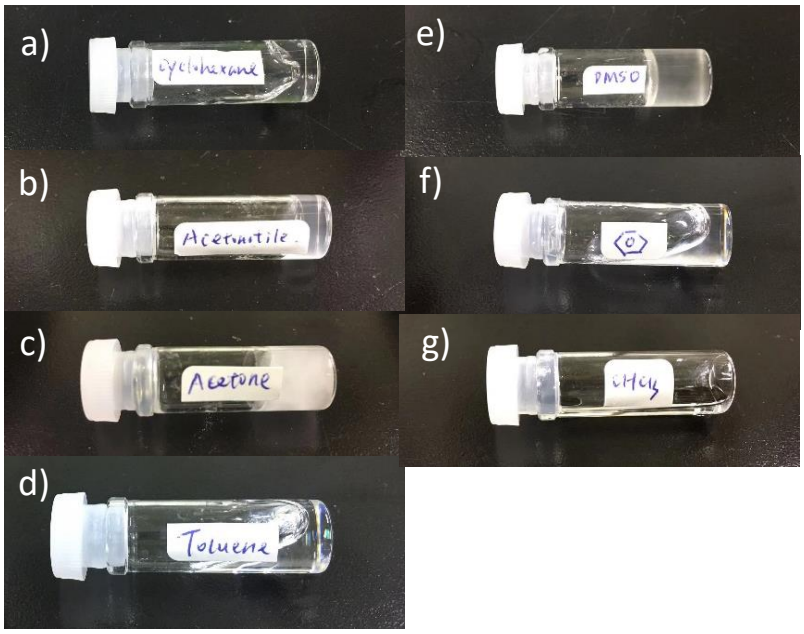

Figure S3. Photographs of molecular assembly of ***S*-3BC** in a) cyclohexane, b) acetonitrile, c) acetone, d) toluene, e) DMSO, f) benzene, and g) $CHCl_3$.

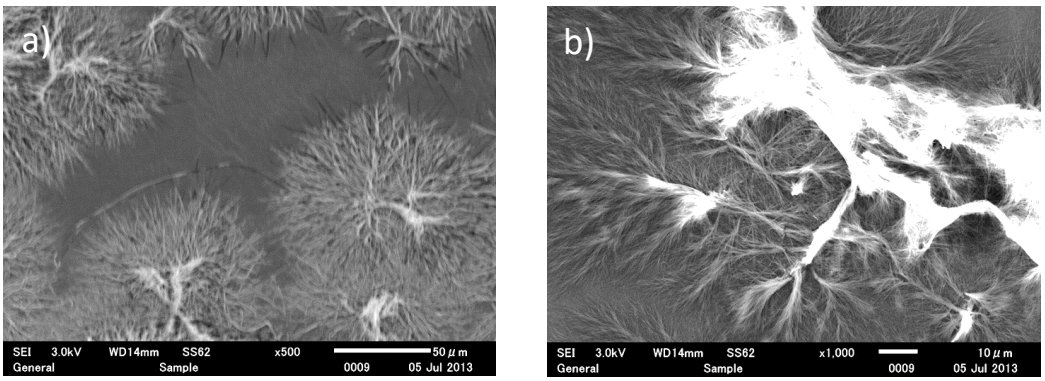

Figure S4. SEM images of xerogels of ***S*-3BC** on HOPG substrate surface, fabricated by the spin-coat technique. Scale-bar of a) 50 and b) 10 μm, respectively.

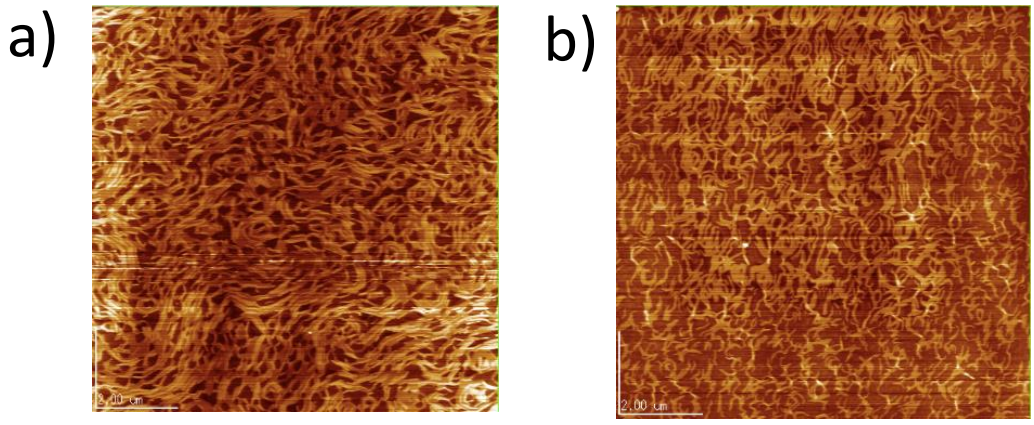

Figure S5. AFM images of xerogels of ***S*-3BC** on mica surface, fabricated by the spin-coat technique of toluene solution with a fixed concentration of 20 mM. Rotation speed of spinner at a) 500 and b) 1000 rpm, respectively. Scale-bar is 2 μm.

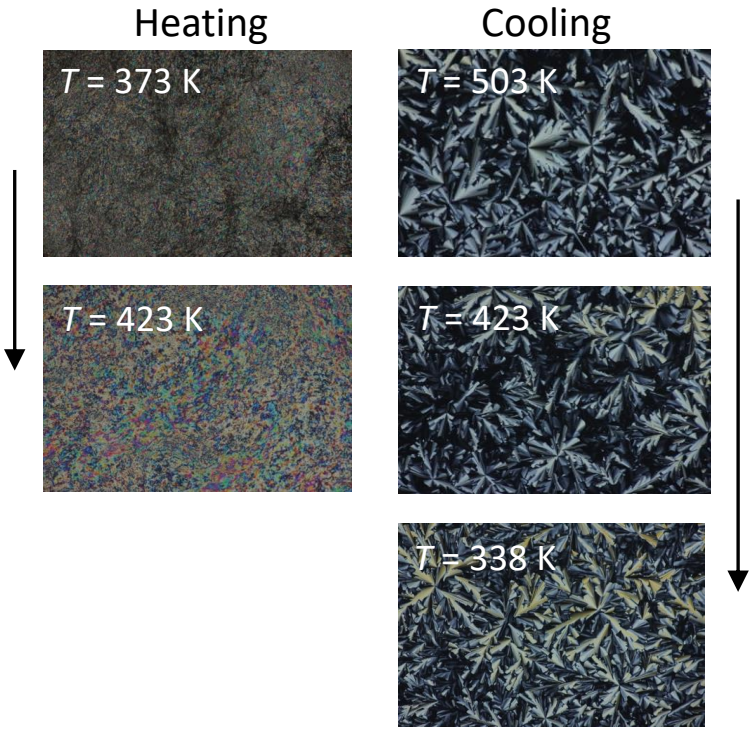

Figure S6. Temperature-dependent texture changes of the POM observation in the heating and cooling processes under the cross-Nicol optical arrangement.

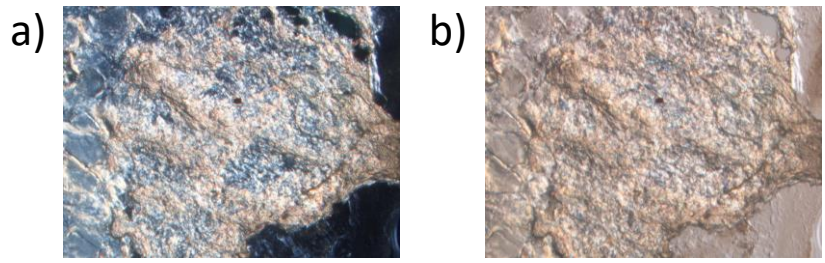

Figure S7. POM images of lyotropic liquid crystal phase in toluene at 298 K with a fixed concentration of 20 mM.

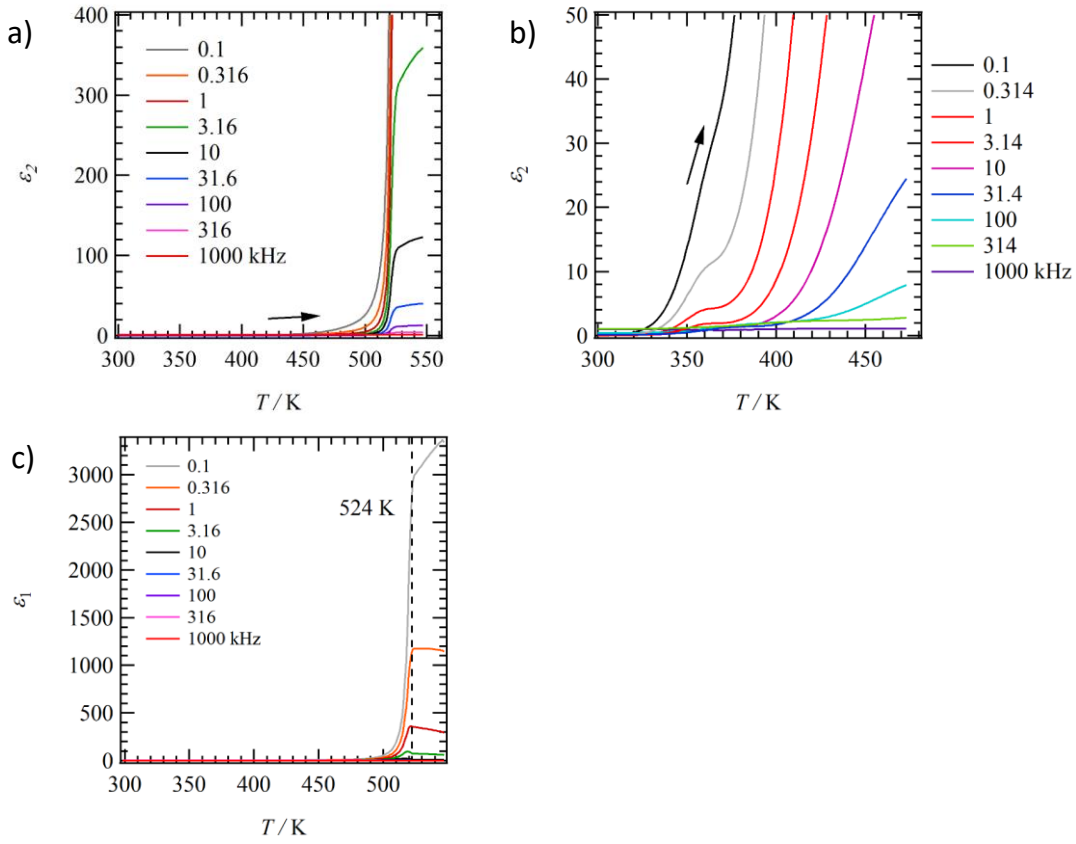

Figure S8. *T*- and *f*-dependent imaginary parts dielectric constants ε_2 of **S-3BC**. a) Overall ε_2-responses to clarify the Col_h – IL phase transition and b) the expanded ε_2-response to clarify the S – Col_h phase transition.

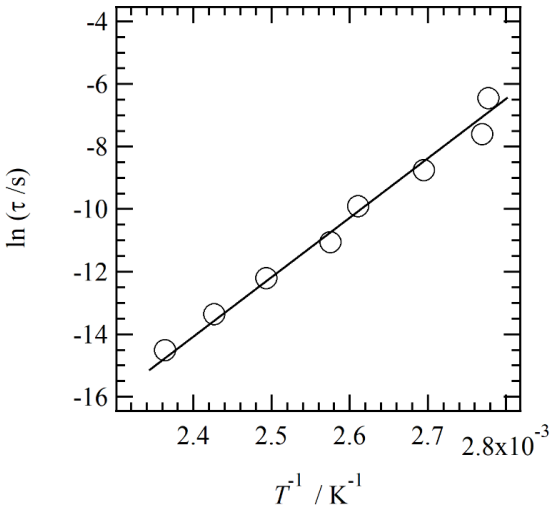

Figure S9. ln (τ) – T_{p1}^{-1} plots of ***S*-3BC**, where the τ-value was a relaxation time of the inverse of measurement *f*-values of the $\tau = 1/(2\pi f)$.

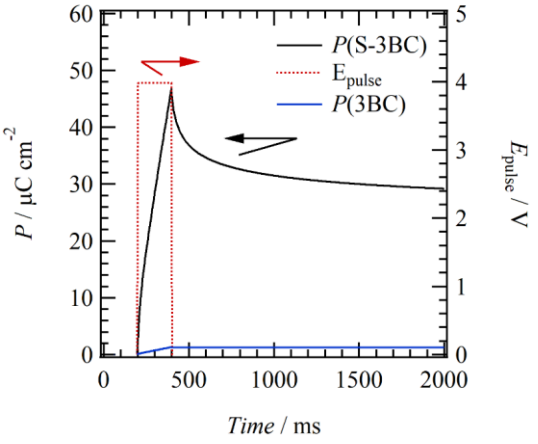

Figure S10. Time-dependent polarization decay of ***S*-3BC** (black) and **3BC** (blue) after the pulse voltage application (red).

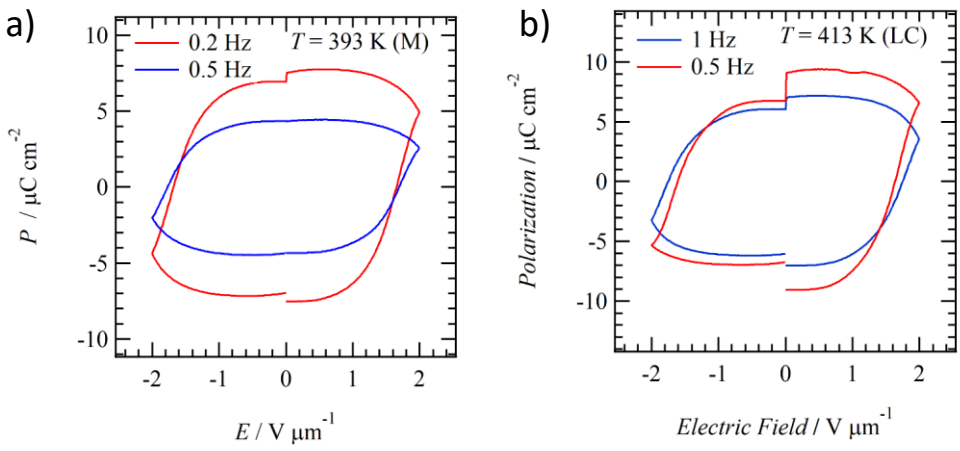

Figure S11. Remanant polarization *P* – *E* hysteresis curve of **3BC** a) at 393 K with *f* = 0.2 and 0.5 Hz and b) at 414 K with *f* = 1 and 0.5 Hz.

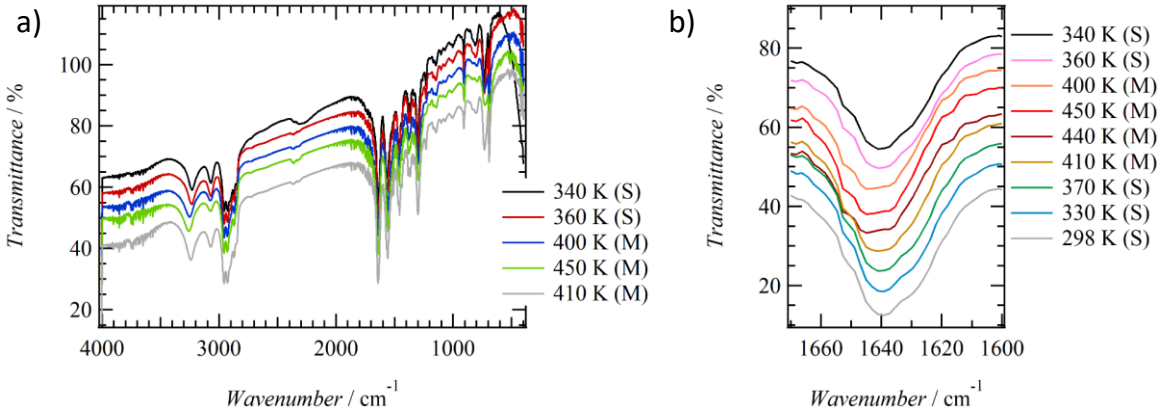

Figure S12. *T*-dependent IR spectra of ***S*-3BC** at the energy range of a) 400 ~ 4000 cm^{-1} and b) 1600 ~ 1700 cm^{-1}.

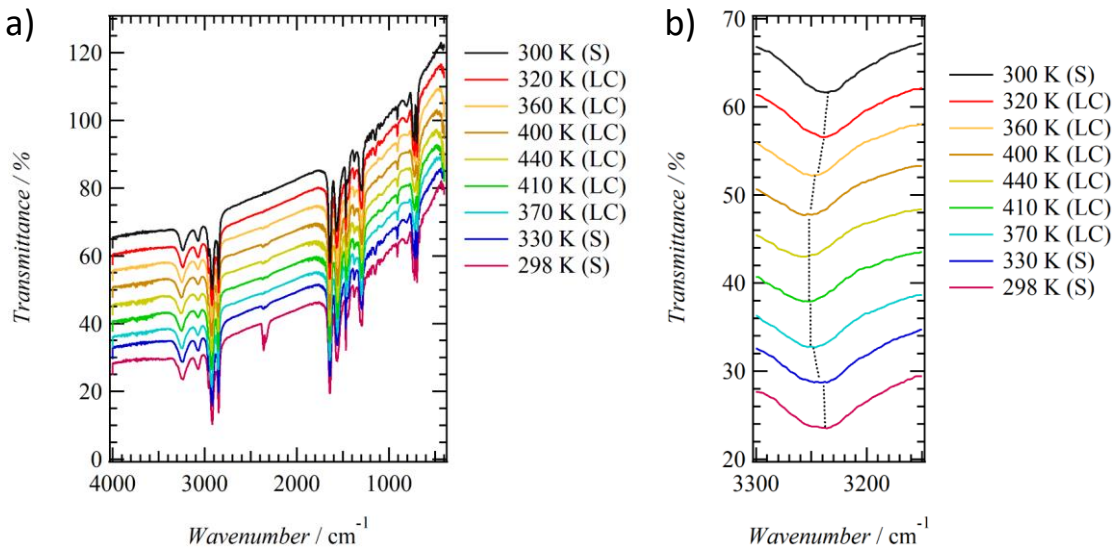

Figure S13. *T*-dependent IR spectra of **3BC** at the energy range of a) 400 ~ 4000 cm^{-1} and b) 3100 ~ 3300 cm^{-1}.